

Optimal superconductivity near a Lifshitz transition in strained $(\text{La},\text{Pr})_3\text{Ni}_2\text{O}_7$

Siheon Ryee,^{1,2,*} Niklas Witt,³ Giorgio Sangiovanni,³ and Tim O. Wehling^{1,2}

¹*Institute of Theoretical Physics, University of Hamburg, Notkestraße 9-11, 22607 Hamburg, Germany*

²*The Hamburg Centre for Ultrafast Imaging, Luruper Chaussee 149, 22761 Hamburg, Germany*

³*Institut für Theoretische Physik und Astrophysik and Würzburg-Dresden Cluster*

of Excellence ct.qmat, Universität Würzburg, 97074 Würzburg, Germany

(Dated: June 27, 2025)

High-temperature superconductivity in pressurized and strained bilayer nickelates $(\text{La},\text{Pr})_3\text{Ni}_2\text{O}_7$ has emerged as a new frontier. One of the key unresolved issues concerns the fermiology that underlies superconductivity. On both theoretical and experimental sides, no general consensus has been reached, and conflicting results exist regarding whether the relevant Fermi surface involves a hole γ pocket, or not. Here, we address this issue by unveiling a Janus-faced role of the γ pocket in spin-fluctuation-mediated superconductivity. We show that this pocket simultaneously induces dominant pair-breaking and pair-forming fluctuations for the leading s_{\pm} -wave pairing. Consequently, an optimal superconducting transition temperature T_c is achieved when the γ pocket surfaces at the Fermi level, placing the system near a Lifshitz transition. This suggests that superconductivity can emerge provided the maximum energy level of the γ pocket lies sufficiently close to the Fermi level, either from below or above. Our finding not only reconciles two opposing viewpoints on the fermiology, but also naturally explains recent experiments on $(\text{La},\text{Pr})_3\text{Ni}_2\text{O}_7$ thin films, including the superconductivity under compressive strain, two conflicting measurements on the Fermi surface, and the dome shape of T_c as a function of hole doping.

The discovery of high-temperature superconductivity in pressurized bilayer nickelate $\text{La}_3\text{Ni}_2\text{O}_7$ has opened a new frontier in superconductivity research [1]. This material features bilayer square lattice as a building block [Fig. 1(a)], where three electrons are distributed across four $\text{Ni}-e_g$ orbitals in the top and bottom layers, while fully occupied $\text{Ni}-t_{2g}$ orbitals remain inert to low-energy physics [1–7]. At ambient pressure, $\text{La}_3\text{Ni}_2\text{O}_7$ exhibits a (spin) density wave order below 140 K, and the associated transition temperature is gradually decreased with increasing pressure [8–11]. Above a critical pressure of ~ 10 GPa, superconductivity sets in, reaching a maximum critical temperature $T_c^{\max} \simeq 80$ K near 20 GPa [1, 12–16]. This pressure-induced superconductivity is also observed in its isostructural sibling compounds $\text{La}_2\text{PrNi}_2\text{O}_7$ [17] and $\text{La}_2\text{SmNi}_2\text{O}_{7-\delta}$ [18], and related cousin systems including trilayer nickelate $\text{La}_4\text{Ni}_3\text{O}_{10}$ [19–21], alternately stacked trilayer–monolayer polymorph of $\text{La}_3\text{Ni}_2\text{O}_7$ [22–24], and $\text{La}_5\text{Ni}_3\text{O}_{11}$ [25].

Despite extensive studies [3–7, 19, 26–74], no general consensus has been reached on fundamental aspects of superconductivity, including the pairing mechanism, gap symmetry, and underlying fermiology. A prevailing view is that strong magnetic interactions or fluctuations play a central role in the emergence of superconductivity in this multilayer nickelate family [5, 7, 19, 27–36, 39–43, 45–54, 63–68, 74, 75]. In this line of thought, there is an issue of whether or not the “flat” γ Fermi surface (FS) pocket centered at the M point of the first Brillouin zone (FBZ) [Fig. 1(b)] exists in the normal state. This question is deeply linked to whether the γ pocket is the main driver of the pairing fluctuations within the spin-fluctuation theory. Although the common belief is that the γ pocket is present and mediates pairing [1, 7, 29, 32–35, 42, 47–51, 54, 66, 67, 74, 75], there are different perspectives challenging this viewpoint [6, 45, 70, 76]. This controversy over “three vs two FS pockets” remains unresolved, partly because

high pressure limits the use of many experimental probes.

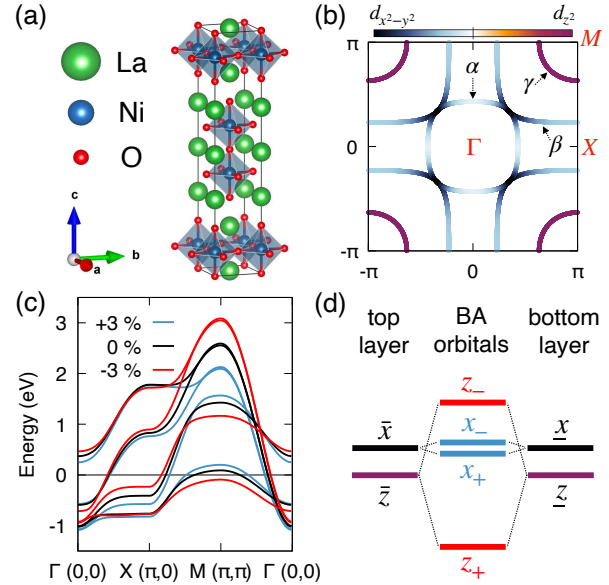


FIG. 1. (a) Crystal structure of $\text{La}_3\text{Ni}_2\text{O}_7$ drawn using VESTA [77]. (b) Fermi surface obtained from the MLWF fit of the DFT band structure at zero strain. The color bar indicates the relative orbital weight. (c) The evolution of the band structure with strain. + and – denote tensile and compressive strain, respectively. (d) Schematic illustration of the formation of BA orbitals from $\text{Ni}-e_g$ orbitals in the top and bottom layers.

In this respect, the recent discovery of superconductivity in thin films of $\text{La}_3\text{Ni}_2\text{O}_7$ [78] and $\text{La}_2\text{PrNi}_2\text{O}_7$ [79, 80] under ambient pressure offers a promising avenue for resolving the issues by enabling application of a broad range of experimental techniques. The key findings are that superconductivity with $T_c \simeq 42$ K or higher emerges in compressively

strained samples (-2% strained thin films on SrLaAlO₄ substrate [78–80]), and samples with smaller in-plane Ni–O bond length have higher T_c [78]. These are striking observations, because the standard *ab initio* calculations based on density functional theory (DFT) unequivocally point out that compressive strain suppresses the γ pocket [81–83]; see Fig. 1(c). Interestingly, recent angle-resolved photoemission spectroscopy (ARPES) measurements have reported conflicting results regarding the presence of the γ pocket [84, 85]. Taken together, these findings revive the central issue concerning the presence of the γ pocket and its role in spin-fluctuation-mediated superconductivity.

In this work, we solve this problem by identifying a *Janus-faced* role of the γ pocket in the superconductivity of strained bilayer nickelate (La,Pr)₃Ni₂O₇. Namely, the γ pocket simultaneously generates both strong pair-forming and pair-breaking fluctuations, so a delicate balance between them is the key to superconductivity. As a consequence, maximum T_c can be achieved when the γ pocket has just surfaced at the Fermi level, thereby being in proximity to a Lifshitz transition. Our finding not only reconciles two seemingly contradicting perspectives on the fermiology (i.e., three vs two pockets), but also accounts for experimental observations in strained samples, including the enhancement of T_c with increased compressive strain [78, 86], the presumably s_{\pm} -wave gap symmetry [87], conflicting ARPES measurements on the Fermi surface [84, 85], and the dome shape of T_c as a function of hole doping [88].

We first perform DFT calculations and then use the maximally localized Wannier function (MLWF) method [89] to construct a four-orbital (top-layer two Ni- e_g + bottom-layer two Ni- e_g) bilayer square-lattice model of strained La₃Ni₂O₇ using DFT-optimized lattice constants reported in Ref. [81]. Since in-plane lattice constants only differ by about 1% in the orthorhombic Fmmm structure [81, 86], we use higher-symmetry tetragonal I4/mmm structure by averaging the in-plane lattice constants. Atomic positions are relaxed for each lattice constant using the Perdew–Burke–Ernzerhof (PBE) exchange-correlation functional for the generalized gradient approximation [90]. We used the Vienna Ab initio Simulation Package (VASP) [91–93] for DFT calculations and Wannier90 code [94] for constructing MLWFs; see Supplementary for details [95]. The FS and band structures in Figs. 1(b–c) were obtained following this procedure.

To investigate the superconducting phase transition, we use the random phase approximation (RPA) and solve the gap equation given by

$$\lambda_{sc} \Delta_{l_1 l_2}(k) = -\frac{T}{2N} \sum_{q, l_1 l_2 l_3 l_4} \Gamma_{l_1 l_4 l_3 l_2}^{s/t}(q) \times G_{l_4 l_5}(k-q) G_{l_3 l_6}(q-k) \Delta_{l_5 l_6}(k-q), \quad (1)$$

where $k \equiv (\mathbf{k}, i\omega_n)$ and $q \equiv (\mathbf{q}, iv_n)$ with \mathbf{k} and \mathbf{q} being the crystal momentum and ω_n (v_n) the fermionic (bosonic) Matsubara frequency. T is temperature, N the number of q -points in the FBZ, $G(k)$ the bare Green's function, and $\Delta(k)$ the gap

function. $\Gamma_{l_1 l_4 l_3 l_2}^{s/t}(q)$ describe the effective singlet (s) or triplet (t) pairing interaction accounting for scattering of electrons in orbitals (l_1, l_2) with four-momenta $(k, -k)$ to (l_3, l_4) with $(k-q, -k+q)$. In the case of singlet pairing, for instance, the pairing interaction reads [96]

$$\Gamma^s(q) = \frac{3\Gamma^{sp}}{2} + \frac{\Gamma^{ch}}{2} + 3\Gamma^{sp}\chi^{sp}(q)\Gamma^{sp} - \Gamma^{ch}\chi^{ch}(q)\Gamma^{ch}, \quad (2)$$

where $\chi^{sp/ch}$ are the spin (sp) and charge (ch) susceptibilities and $\Gamma^{sp/ch}$ the corresponding vertices (bold symbols will be used to denote matrices). $\chi^{sp/ch}(q) = \chi^0(q)[\mathbf{1} \mp \Gamma^{sp/ch}\chi^0(q)]^{-1}$ where $\mathbf{1}$ is the identity matrix and $\chi^0(q)$ the irreducible susceptibility, whose elements are given by

$$\chi_{l_1 l_2 l_3 l_4}^0(q) = -\frac{T}{N} \sum_k G_{l_1 l_3}(k+q) G_{l_4 l_2}(k). \quad (3)$$

$\Gamma^{sp/ch}$ are constructed from the onsite Kanamori Hamiltonian for the e_g manifold (including intraorbital onsite Coulomb repulsion U , Hund's coupling J , and the interorbital onsite Coulomb repulsion $U' = U - 2J$) and the interlayer density-density interaction V [95]. The phase transition to the superconducting state is indicated by the temperature T_c at which the maximum eigenvalue λ_{sc} reaches unity. Thus, λ_{sc} serves as a proxy for the superconducting instability. We investigate the leading λ_{sc} at a fixed $T = 1/140$ eV $\simeq 83$ K. To avoid divergence of the dominant spin susceptibility while ensuring a sizable λ_{sc} , we choose an interaction strength of $U = 0.96$ eV and set $J = U/6$ and $V = 0$ for the main discussion. Note that we use the RPA here to assess strain and doping dependence of superconducting instabilities, their leading pairing symmetry, and the role of the fermiology, but not to quantitatively predict T_c . See Supplementary for more details [95].

Our main result is presented in the bottom panel of Fig. 2(a) which shows the maximum λ_{sc} as a function of strain at an average electron filling of 3. We find that the instability to singlet pairing dominates over that to triplet pairing, and the maximum eigenvalue of χ^{sp} is much larger than that of χ^{ch} indicating that the singlet pairing is mediated by spin fluctuations. The dominant pairing symmetry for the compressive-strain side is s_{\pm} where the gap changes sign between neighboring FS pockets [95]. This is consistent with the experiment on the -2% strained sample, supporting the s_{\pm} over d -wave gap symmetries [87], and aligns with a recent theoretical study reporting the robustness of the s_{\pm} -wave pairing [97]. While we find that the instability to the $d_{x^2-y^2}$ -wave paring dominates over that to the s_{\pm} -wave on some tensile strains, they are comparable in magnitude. This superconductivity–strain profile remains unaffected by variations in the interaction strength; see Supplementary for additional data [95].

Most notably, Fig. 2(a) demonstrates that superconductivity is promoted by compressive strain, not by tensile strain, in agreement with experiments [78–80, 86]. This is a surprising outcome since the prevailing theoretical picture has been that the γ pocket—which gets bigger with *tensile* strain [as presented in the top panel of Fig. 2(a)]—promotes spin-fluctuation-mediated superconductivity [1, 7, 29, 32–35, 42, 47–51, 54,

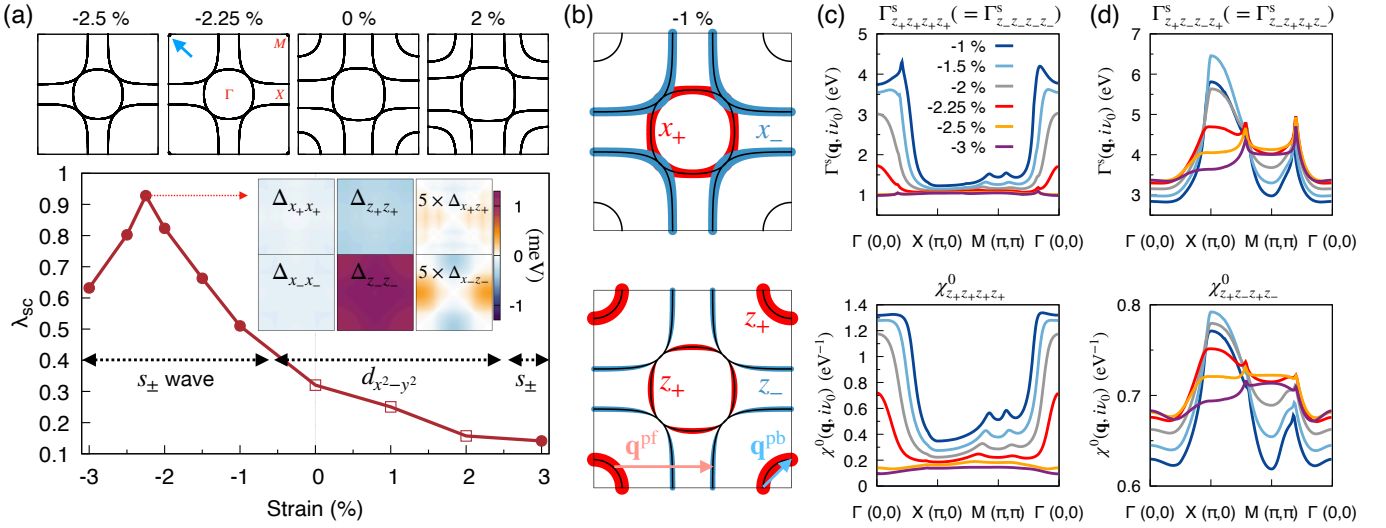


FIG. 2. (a) The leading λ_{sc} as a function of strain (bottom) and the FSs for several values of strain (top). The blue arrow in the top panel highlights the marginal presence of the γ pocket at -2.25% strain. The inset in the bottom panel shows the nonzero elements of $\Delta_{lm}(\mathbf{k}, i\omega_0)$ in the BA basis at -2.25% strain. Circles: s_\pm -wave gap; squares: $d_{x^2-y^2}$ -wave gap. (b) Orbital weight on the FS at -1% strain. The top panel shows the x_+ and x_- contributions and the bottom panel shows the z_+ and z_- contributions. $\mathbf{q}^{pf} = (\epsilon_1, \epsilon_2)$ with $\epsilon_1, \epsilon_2 < \pi$ being small numbers, and $\mathbf{q}^{pb} = (\pi, 0)$ denote nesting vectors associated with the pair-breaking and pair-forming channels, respectively, for the s_\pm -wave pairing. (c) The pair-breaking interaction $\Gamma_{z_+z_+z_+z_+}^s(\mathbf{q}, i\omega_0) \{= \Gamma_{z_-z_-z_-z_-}^s(\mathbf{q}, i\omega_0)\}$ (top) and the associated irreducible susceptibility $\chi_{z_+z_+z_+z_+}^0(\mathbf{q}, i\omega_0)$ (bottom). (d) The pair-forming interaction $\Gamma_{z_+z_-z_-z_+}^s(\mathbf{q}, i\omega_0) \{= \Gamma_{z_-z_+z_+z_-}^s(\mathbf{q}, i\omega_0)\}$ (top) and the associated irreducible susceptibility $\chi_{z_+z_-z_-z_+}^0(\mathbf{q}, i\omega_0)$ (bottom).

[66, 67, 74, 75]. Furthermore, λ_{sc} reaches its maximum at -2.25% strain, where the γ pocket is marginally present at the M point [FS shown in the top panel of Fig. 2(a)].

To systematically trace the origin of this result, we first switch to the bonding-antibonding (BA) orbital basis as schematically shown in Fig. 1(d). We denote $d_{x^2-y^2}$ orbital by x and d_{z^2} by z for simplicity. The BA orbitals are defined by the + and - linear combinations of the top and bottom layer e_g orbitals: $|\eta_\pm\rangle = (|\bar{\eta}\rangle \pm |\eta\rangle)/\sqrt{2}$, where ket symbols indicate the corresponding MLWF orbitals. $\bar{\eta}$ and η represent Ni- e_g orbitals ($\eta \in \{x, z\}$) in the top and bottom layers, respectively. A clear advantage of using this basis is that the BA orbitals for each type are orthogonal ($\langle \eta_+ | \eta_- \rangle = 0$), and the γ pocket consists entirely of the z_+ orbital character [Fig. 2(b)].

A strikingly simple structure of the s_\pm -wave gap function emerges in the BA basis. As shown in the inset of Fig. 2(a) for -2.25% strain, it exhibits significant magnitude only in the $\Delta_{z_+z_+}$ and $\Delta_{z_-z_-}$ components with opposite signs, indicating strong *interlayer* pairing between the top and bottom layer z orbitals. This observation allows us to simplify Eq. (1) as

$$\begin{aligned} \lambda_{sc} \Delta_{z_+z_+}(k) &\simeq -\Gamma_{z_+z_+z_+z_+}^s(q) |G_{z_+z_+}(k-q)|^2 \Delta_{z_+z_+}(k-q) \\ &\quad - \Gamma_{z_+z_-z_-z_+}^s(q) |G_{z_-z_-}(k-q)|^2 \Delta_{z_-z_-}(k-q), \\ \lambda_{sc} \Delta_{z_-z_-}(k) &\simeq -\Gamma_{z_-z_-z_-z_-}^s(q) |G_{z_-z_-}(k-q)|^2 \Delta_{z_-z_-}(k-q) \\ &\quad - \Gamma_{z_-z_+z_+z_-}^s(q) |G_{z_+z_+}(k-q)|^2 \Delta_{z_+z_+}(k-q), \end{aligned} \quad (4)$$

with the summation over q and the associated prefactor $T/2N$ understood to be implicit on the right-hand sides of Eq (4). The

pairing interactions appearing in Eq. (4) are all positive definite as shown in the top panels of Figs. 2(c, d) for the lowest bosonic Matsubara frequency $\nu_0 = 0$. Furthermore, exploiting the relation between Γ^s [Eq. (2)] and χ^0 [Eq. (3)], and noting that the spin susceptibility dominates over charge susceptibility, the relevant Γ^s components can be expanded up to second order in interactions as [95]

$$\begin{aligned} \Gamma_{z_+z_+z_+z_+}^s(q) &= \Gamma_{z_-z_-z_-z_-}^s(q) \simeq U + \frac{3}{4} U^2 \chi_{z_+z_+z_+z_+}^0(q), \\ \Gamma_{z_+z_-z_-z_+}^s(q) &= \Gamma_{z_-z_+z_+z_-}^s(q) \simeq U + \frac{3}{2} U^2 \chi_{z_+z_-z_-z_+}^0(q), \end{aligned} \quad (5)$$

where terms containing UJ and J^2 are dropped since $J \ll U$, and the term $(3U^2/4)\chi_{z_-z_-z_-z_-}^0$ is neglected in the first line of Eq. (5) because $\chi_{z_-z_-z_-z_-}^0 \ll \chi_{z_+z_+z_+z_+}^0$; see Supplementary for more details [95].

The approximate gap equation [Eq. (4)] along with Eq. (5) provides key insight: To maximize λ_{sc} , the first terms on the right-hand side of Eq. (4) should be minimized, while the second terms are maximized, since $\Delta_{z_+z_+} < 0$ and $\Delta_{z_-z_-} > 0$ over the FBZ. As a result, $\Gamma_{z_+z_+z_+z_+}^s$ and $\Gamma_{z_-z_-z_-z_-}^s$ appearing in the first terms act as pair-breaking interactions, whereas $\Gamma_{z_+z_-z_-z_+}^s$ and $\Gamma_{z_-z_+z_+z_-}^s$ in the second terms serve as pair-forming interactions for the s_\pm -wave pairing. From Eq. (5), we therefore identify $\chi_{z_+z_+z_+z_+}^0$ and $\chi_{z_+z_-z_-z_+}^0$ as the main pair-breaking and pair-forming fluctuations, respectively. Figures 2(c, d) indeed show essentially the same momentum dependence of these χ^0 elements as that of the associated pairing interactions. The maxima of both the pair-breaking [Fig. 2(c)]

and pair-forming [Fig. 2(d)] channels tend to decrease with increasing compressive strain. At -2.25% strain where λ_{sc} reaches its maximum, the pair-breaking channel is largely (but not completely) suppressed, while the pair-forming channel remains moderate.

An important finding is that the γ pocket promotes both the dominant pair-breaking and pair-forming channels, thereby exhibiting a dual nature. Namely, this pocket simultaneously gives rise to the two distinct nesting vectors as illustrated in Fig. 2(b): $q^{pb} = (\epsilon_1, \epsilon_2)$ with $\epsilon_1, \epsilon_2 < \pi$ being small numbers and $q^{pf} = (\pi, 0)$, which are responsible for the pair-breaking ($\chi_{z_+z_+z_+z_+}^0$) and pair-forming ($\chi_{z_+z_+z_+z_-}^0$) fluctuations, respectively. As the γ pocket shrinks with increasing compressive strain, the pair-breaking channel $\chi_{z_+z_+z_+z_+}^0$ is progressively suppressed due to the reduced phase space available for particle-hole fluctuations with $q \simeq q^{pb}$ within the γ pocket. Once the γ pocket completely disappears from the FS (e.g., -2.5 and -3% strains), $\chi_{z_+z_+z_+z_+}^0$ becomes almost entirely quenched [Fig. 2(c)]. Likewise, the maximum of the pair-forming $\chi_{z_+z_-z_+z_-}^0$ is progressively reduced with increasing compressive strain, and eventually loses fluctuation with $q \simeq q^{pf}$ connecting the γ and β pockets once the former vanishes from the FS [Fig. 2(d)]. Thus, in order to achieve both a sufficiently small pair-breaking $\chi_{z_+z_+z_+z_+}^0$ and a sufficiently large pair-forming $\chi_{z_+z_-z_+z_-}^0$, a marginal presence of the γ pocket turns out to be optimal. This explains why λ_{sc} reaches its maximum at -2.25% strain as in Fig. 2(a), and highlights that a delicate balance between the two opposing channels via size of the γ pocket is essential for optimizing T_c . Our picture may have some relevance to the so-called “incipient band” scenario suggested in the context of iron-based superconductors or bilayer Hubbard models [98–102]. Understanding of their connection requires further study.

It should be noted that the presence of the γ pocket in the FS is not a prerequisite for superconductivity in $(La,Pr)_3Ni_2O_7$. As shown in Fig. 2(a), the two-pocket FS realized for a larger compressive strain (-2.5%) yields a sizable value of λ_{sc} . In fact, λ_{sc} exhibits an almost symmetric profile with respect to its peak at -2.25% strain, as shown in Fig. 2(a). Therefore, superconductivity can emerge provided the “valence-band maximum” of the γ pocket lies sufficiently close to the Fermi level, either from below or above. This finding not only reconciles two opposing viewpoints regarding which fermiology (i.e., three vs two pockets) underlies superconductivity [1, 6, 7, 29, 32–35, 42, 45, 47–51, 54, 66, 67, 70, 74, 75], but also explains conflicting ARPES measurements that report the presence [84] and absence [85] of the γ pocket in compressively strained $(La,Pr)_3Ni_2O_7$ thin films exhibiting superconductivity.

On the tensile strain side, a sizable γ pocket leads to an enhanced $\chi_{z_+z_+z_+z_+}^0$ and thus $\Gamma_{z_+z_+z_+z_+}^s$ which significantly suppresses the s_{\pm} -wave pairing and instead promotes the $d_{x^2-y^2}$ -wave pairing as the leading instability. However, due to the small λ_{sc} on the tensile-strain side [Fig. 2(a)], an actual phase transition to superconductivity seems unlikely here.

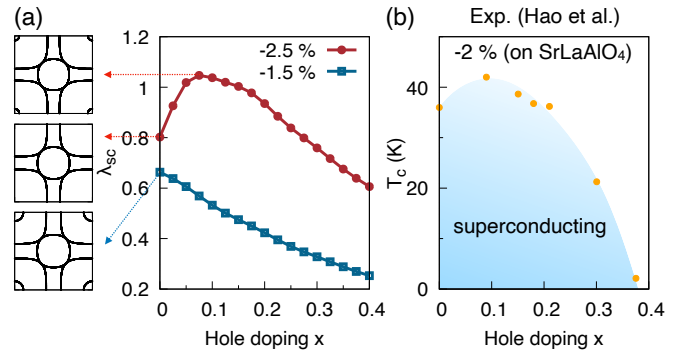


FIG. 3. (a) λ_{sc} as a function of hole doping x for -2.5% and -1.5% strains (right), and the corresponding FSs for selected cases (left). (b) Experimental phase diagram of -2% strained $La_{3-x}Sr_xNi_2O_7$ thin films grown on $SrLaAlO_4$ substrate with x denoting hole doping. The yellow circles are the experimental data at which the resistivity reaches 98 % of the extrapolated normal-state resistivity [88].

Having established the relationship between fermiology and superconducting instabilities as a function of strain, we now turn to the effect of doping. An interesting recent experimental observation [88] is that T_c forms a dome shape as a function of hole doping x in $La_{3-x}Sr_xNi_2O_7$ thin films grown on $SrLaAlO_4$ substrate; see Fig. 3(b). At an optimal hole doping of $x = 0.09$, T_c reaches its maximum with $T_c \simeq 42$ K [88]. Motivated by this observation, we investigate the superconducting instability as a function of hole doping. To this end, we simply shift the chemical potential to achieve the desired doping level with the underlying MLWF band structure remaining unchanged at a given strain.

Figure 3(a) shows the calculated λ_{sc} as a function of hole doping at two different compressive strains. The leading instability remains also the s_{\pm} -wave pairing for the entire doping range. Interestingly, two distinct doping dependencies emerge, depending on whether the γ pocket is present at zero hole doping ($x = 0$), or not. While λ_{sc} monotonically decreases with hole doping at -1.5% strain, it initially increases and then decreases with doping at -2.5% strain forming a maximum at $x = 0.075$. This doping dependence in the -2.5% strain case is in agreement with the experiment [88] shown in Fig. 3(b). Here as well, the maximum of λ_{sc} occurs when the γ pocket is marginally present in the FS, as shown in the top left panel of Fig. 3(a). Enlarging the γ pocket by further hole doping is detrimental to superconductivity, as it enhances the pair-breaking fluctuation $\chi_{z_+z_+z_+z_+}^0$; see Supplementary for additional data and for data on the electron-doped region [95]. Thus, despite the simplified nature of our model, the proposed picture that T_c is optimal when the γ pocket slightly crosses the Fermi level near a Lifshitz transition accounts for the overall trend of the experimental hole-doping dependence.

To conclude, we have established the Janus-faced role of the γ pocket in spin-fluctuated-mediated superconductivity of strained bilayer nickelates. Our finding reconciles two seemingly contradicting perspectives on the fermiology (i.e., three vs two FS pockets), as well as accounts for several recent

experimental observations in strained samples under ambient pressure. Very recently, an experiment on pressurized $\text{La}_3\text{Ni}_2\text{O}_7$ thin films reported superconductivity even under tensile strain at high pressures ($>\sim 10 \text{ GPa}$) [103]. Although the γ pocket remains sizable under tensile strain [Fig. 2(a)], pressure can lead to a shrinking, or even quenching of the γ pocket, assisted by interlayer electronic correlations [45]. We thus expect that the mechanism proposed in the present work can also be applied to this experimental finding.

A natural consequence of our picture is that optimal T_c is achieved when the γ pocket surfaces at the Fermi level, placing the system close to a Lifshitz transition. This calls for future experimental investigations, and serves as a guiding principle for realizing higher T_c . Establishing a unified framework of superconductivity that encompasses both strain and pressure dependence in the multilayer nickelate family remains an outstanding challenge, which requires more quantitative and sophisticated theoretical approaches. The present work offers a conceptual basis for this endeavor.

Acknowledgments. SR and TOW acknowledge funding and support by the DFG research unit FOR 5242 (WE 5342/7-1, project No. 449119662), and from the Cluster of Excellence “CUI: Advanced Imaging of Matter” of the DFG (EXC 2056, Project ID 390715994). NW and GS acknowledge funding and support by the DFG research unit FOR 5249 (“QUAST”, project No. 449872909) and the DFG funded SFB 1170 (“Toctronics”, project No. 258499086).

* siheon.ryee@uni-hamburg.de

- [1] H. Sun, M. Huo, X. Hu, J. Li, Z. Liu, Y. Han, L. Tang, Z. Mao, P. Yang, B. Wang, J. Cheng, D.-X. Yao, G.-M. Zhang, and M. Wang, *Nature* **621**, 493 (2023), number: 7979 Publisher: Nature Publishing Group.
- [2] J. Yang, H. Sun, X. Hu, Y. Xie, T. Miao, H. Luo, H. Chen, B. Liang, W. Zhu, G. Qu, C.-Q. Chen, M. Huo, Y. Huang, S. Zhang, F. Zhang, F. Yang, Z. Wang, Q. Peng, H. Mao, G. Liu, Z. Xu, T. Qian, D.-X. Yao, M. Wang, L. Zhao, and X. J. Zhou, *Nature Communications* **15**, 4373 (2024).
- [3] Z. Luo, X. Hu, M. Wang, W. Wú, and D.-X. Yao, *Physical Review Letters* **131**, 126001 (2023), publisher: American Physical Society.
- [4] Y. Gu, C. Le, Z. Yang, X. Wu, and J. Hu, *Phys. Rev. B* **111**, 174506 (2025).
- [5] Y. Shen, M. Qin, and G.-M. Zhang, *Chinese Physics Letters* **40**, 127401 (2023).
- [6] V. Christiansson, F. Petocchi, and P. Werner, *Phys. Rev. Lett.* **131**, 206501 (2023).
- [7] Y. Zhang, L.-F. Lin, A. Moreo, T. A. Maier, and E. Dagotto, *Phys. Rev. B* **108**, 165141 (2023).
- [8] Z. Liu, H. Sun, M. Huo, X. Ma, Y. Ji, E. Yi, L. Li, H. Liu, J. Yu, Z. Zhang, Z. Chen, F. Liang, H. Dong, H. Guo, D. Zhong, B. Shen, S. Li, and M. Wang, *Science China Physics, Mechanics & Astronomy* **66**, 217411 (2022).
- [9] K. Chen, X. Liu, J. Jiao, M. Zou, C. Jiang, X. Li, Y. Luo, Q. Wu, N. Zhang, Y. Guo, and L. Shu, *Phys. Rev. Lett.* **132**, 256503 (2024).
- [10] X. Chen, J. Choi, Z. Jiang, J. Mei, K. Jiang, J. Li, S. Agrestini, M. Garcia-Fernandez, H. Sun, X. Huang, D. Shen, M. Wang, J. Hu, Y. Lu, K.-J. Zhou, and D. Feng, *Nature Communications* **15**, 9597 (2024).
- [11] R. Khasanov, T. J. Hicken, D. J. Gawryluk, V. Sazgari, I. Plokhikh, L. P. Sorel, M. Bartkowiak, S. Böttzel, F. Lechermann, I. M. Eremin, H. Luetkens, and Z. Guguchia, *Nature Physics* **21**, 430 (2025).
- [12] J. Hou, P.-T. Yang, Z.-Y. Liu, J.-Y. Li, P.-F. Shan, L. Ma, G. Wang, N.-N. Wang, H.-Z. Guo, J.-P. Sun, Y. Uwatoko, M. Wang, G.-M. Zhang, B.-S. Wang, and J.-G. Cheng, *Chinese Physics Letters* **40**, 117302 (2023).
- [13] Y. Zhang, D. Su, Y. Huang, Z. Shan, H. Sun, M. Huo, K. Ye, J. Zhang, Z. Yang, Y. Xu, Y. Su, R. Li, M. Smidman, M. Wang, L. Jiao, and H. Yuan, *Nature Physics* **20**, 1269 (2024).
- [14] G. Wang, N. N. Wang, X. L. Shen, J. Hou, L. Ma, L. F. Shi, Z. A. Ren, Y. D. Gu, H. M. Ma, P. T. Yang, Z. Y. Liu, H. Z. Guo, J. P. Sun, G. M. Zhang, S. Calder, J.-Q. Yan, B. S. Wang, Y. Uwatoko, and J.-G. Cheng, *Phys. Rev. X* **14**, 011040 (2024).
- [15] M. Zhang, C. Pei, Q. Wang, Y. Zhao, C. Li, W. Cao, S. Zhu, J. Wu, and Y. Qi, *Journal of Materials Science & Technology* **185**, 147 (2024).
- [16] J. Li, D. Peng, P. Ma, H. Zhang, Z. Xing, X. Huang, C. Huang, M. Huo, D. Hu, Z. Dong, X. Chen, T. Xie, H. Dong, H. Sun, Q. Zeng, H.-k. Mao, and M. Wang, *National Science Review*, nwaf220 (2025).
- [17] N. Wang, G. Wang, X. Shen, J. Hou, J. Luo, X. Ma, H. Yang, L. Shi, J. Dou, J. Feng, J. Yang, Y. Shi, Z. Ren, H. Ma, P. Yang, Z. Liu, Y. Liu, H. Zhang, X. Dong, Y. Wang, K. Jiang, J. Hu, S. Nagasaki, K. Kitagawa, S. Calder, J. Yan, J. Sun, B. Wang, R. Zhou, Y. Uwatoko, and J. Cheng, *Nature* **634**, 579 (2024).
- [18] F. Li, Z. Xing, D. Peng, J. Dou, N. Guo, L. Ma, Y. Zhang, L. Wang, J. Luo, J. Yang, J. Zhang, T. Chang, Y.-S. Chen, W. Cai, J. Cheng, Y. Wang, Z. Zeng, Q. Zheng, R. Zhou, Q. Zeng, X. Tao, and J. Zhang, *Ambient pressure growth of bilayer nickelate single crystals with superconductivity over 90 k under high pressure* (2025), arXiv:2501.14584 [cond-mat.supr-con].
- [19] H. Sakakibara, M. Ochi, H. Nagata, Y. Ueki, H. Sakurai, R. Matsumoto, K. Terashima, K. Hirose, H. Ohta, M. Kato, Y. Takano, and K. Kuroki, *Phys. Rev. B* **109**, 144511 (2024).
- [20] Y. Zhu, D. Peng, E. Zhang, B. Pan, X. Chen, L. Chen, H. Ren, F. Liu, Y. Hao, N. Li, Z. Xing, F. Lan, J. Han, J. Wang, D. Jia, H. Wo, Y. Gu, Y. Gu, L. Ji, W. Wang, H. Gou, Y. Shen, T. Ying, X. Chen, W. Yang, H. Cao, C. Zheng, Q. Zeng, J.-g. Guo, and J. Zhao, *Nature* **631**, 531 (2024).
- [21] Q. Li, Y.-J. Zhang, Z.-N. Xiang, Y. Zhang, X. Zhu, and H.-H. Wen, *Chinese Physics Letters* **41**, 017401 (2024).
- [22] X. Chen, J. Zhang, A. S. Thind, S. Sharma, H. LaBollita, G. Peterson, H. Zheng, D. P. Phelan, A. S. Botana, R. F. Klie, and J. F. Mitchell, *Journal of the American Chemical Society* **146**, 3640 (2024), pMID: 38294831, <https://doi.org/10.1021/jacs.3c14052>.
- [23] P. Puphal, P. Reiss, N. Enderlein, Y.-M. Wu, G. Khalilullin, V. Sundaramurthy, T. Priessnitz, M. Knauf, A. Suthar, L. Richter, M. Isobe, P. A. van Aken, H. Takagi, B. Keimer, Y. E. Suyolcu, B. Wehinger, P. Hansmann, and M. Hepting, *Phys. Rev. Lett.* **133**, 146002 (2024).
- [24] S. Abadi, K.-J. Xu, E. G. Lomeli, P. Puphal, M. Isobe, Y. Zhong, A. V. Fedorov, S.-K. Mo, M. Hashimoto, D.-H. Lu, B. Moritz, B. Keimer, T. P. Devoreaux, M. Hepting, and Z.-X. Shen, *Phys. Rev. Lett.* **134**, 126001 (2025).
- [25] M. Shi, D. Peng, K. Fan, Z. Xing, S. Yang, Y. Wang, H. Li, R. Wu, M. Du, B. Ge, Z. Zeng, Q. Zeng, J. Ying, T. Wu, and X. Chen, *Superconductivity of the hybrid Ruddlesden-*

- popper la₅ni₃o₁₁ single crystals under high pressure (2025), arXiv:2502.01018 [cond-mat.supr-con].
- [26] D. A. Shilenko and I. V. Leonov, *Physical Review B* **108**, 125105 (2023), publisher: American Physical Society.
- [27] H. Sakakibara, N. Kitamine, M. Ochi, and K. Kuroki, *Phys. Rev. Lett.* **132**, 106002 (2024).
- [28] H. Oh and Y.-H. Zhang, *Phys. Rev. B* **108**, 174511 (2023).
- [29] F. Lechermann, J. Gondolf, S. Bötzsel, and I. M. Eremin, *Phys. Rev. B* **108**, L201121 (2023).
- [30] Z. Liao, L. Chen, G. Duan, Y. Wang, C. Liu, R. Yu, and Q. Si, *Phys. Rev. B* **108**, 214522 (2023).
- [31] Q. Qin and Y.-f. Yang, *Phys. Rev. B* **108**, L140504 (2023).
- [32] C. Lu, Z. Pan, F. Yang, and C. Wu, *Phys. Rev. Lett.* **132**, 146002 (2024).
- [33] Y.-H. Tian, Y. Chen, J.-M. Wang, R.-Q. He, and Z.-Y. Lu, *Phys. Rev. B* **109**, 165154 (2024).
- [34] Q.-G. Yang, D. Wang, and Q.-H. Wang, *Phys. Rev. B* **108**, L140505 (2023).
- [35] D.-C. Lu, M. Li, Z.-Y. Zeng, W. Hou, J. Wang, F. Yang, and Y.-Z. You, *Superconductivity from Doping Symmetric Mass Generation Insulators: Application to La₃Ni₂O₇ under Pressure* (2023), arXiv:2308.11195 [cond-mat].
- [36] W. Wú, Z. Luo, D.-X. Yao, and M. Wang, *Science China Physics, Mechanics & Astronomy* **67**, 117402 (2024).
- [37] H. LaBollita, V. Pardo, M. R. Norman, and A. S. Botana, *Electronic structure and magnetic properties of La₃Ni₂O₇ under pressure* (2023), arXiv:2309.17279 [cond-mat].
- [38] Y. Cao and Y.-f. Yang, *Phys. Rev. B* **109**, L081105 (2024).
- [39] X.-Z. Qu, D.-W. Qu, J. Chen, C. Wu, F. Yang, W. Li, and G. Su, *Phys. Rev. Lett.* **132**, 036502 (2024).
- [40] H. Yang, H. Oh, and Y.-H. Zhang, *Phys. Rev. B* **110**, 104517 (2024).
- [41] Y.-f. Yang, G.-M. Zhang, and F.-C. Zhang, *Phys. Rev. B* **108**, L201108 (2023).
- [42] K. Jiang, Z. Wang, and F.-C. Zhang, *High-temperature superconductivity in la₃ni₂O₇* (2024).
- [43] Y. Zhang, L.-F. Lin, A. Moreo, T. A. Maier, and E. Dagotto, *Nature Communications* **15**, 2470 (2024).
- [44] J. Huang, Z. D. Wang, and T. Zhou, *Phys. Rev. B* **108**, 174501 (2023).
- [45] S. Ryee, N. Witt, and T. O. Wehling, *Phys. Rev. Lett.* **133**, 096002 (2024).
- [46] J.-X. Zhang, H.-K. Zhang, Y.-Z. You, and Z.-Y. Weng, *Phys. Rev. Lett.* **133**, 126501 (2024).
- [47] Z. Fan, J.-F. Zhang, B. Zhan, D. Lv, X.-Y. Jiang, B. Normand, and T. Xiang, *Phys. Rev. B* **110**, 024514 (2024).
- [48] Y. Zhang, L.-F. Lin, A. Moreo, T. A. Maier, and E. Dagotto, *Phys. Rev. Lett.* **133**, 136001 (2024).
- [49] M. Zhang, H. Sun, Y.-B. Liu, Q. Liu, W.-Q. Chen, and F. Yang, *Phys. Rev. B* **110**, L180501 (2024).
- [50] Q.-G. Yang, K.-Y. Jiang, D. Wang, H.-Y. Lu, and Q.-H. Wang, *Phys. Rev. B* **109**, L220506 (2024).
- [51] Y. Zhang, L.-F. Lin, A. Moreo, T. A. Maier, and E. Dagotto, *Phys. Rev. B* **110**, L060510 (2024).
- [52] Y.-f. Yang, *Phys. Rev. B* **110**, 104507 (2024).
- [53] C. Lu, Z. Pan, F. Yang, and C. Wu, *Phys. Rev. B* **110**, 094509 (2024).
- [54] G. Heier, K. Park, and S. Y. Savrasov, *Phys. Rev. B* **109**, 104508 (2024).
- [55] X. Sui, X. Han, H. Jin, X. Chen, L. Qiao, X. Shao, and B. Huang, *Phys. Rev. B* **109**, 205156 (2024).
- [56] B. Geisler, J. J. Hamlin, G. R. Stewart, R. G. Hennig, and P. J. Hirschfeld, *npj Quantum Materials* **9**, 38 (2024).
- [57] L. C. Rhodes and P. Wahl, *Phys. Rev. Mater.* **8**, 044801 (2024).
- [58] H. LaBollita, J. Kapeghian, M. R. Norman, and A. S. Botana, *Phys. Rev. B* **109**, 195151 (2024).
- [59] B. Geisler, L. Fanfarillo, J. J. Hamlin, G. R. Stewart, R. G. Hennig, and P. J. Hirschfeld, *npj Quantum Materials* **9**, 89 (2024).
- [60] H. LaBollita, S. Bag, J. Kapeghian, and A. S. Botana, *Phys. Rev. B* **110**, 155145 (2024).
- [61] F. Lechermann, S. Bötzsel, and I. M. Eremin, *Phys. Rev. Mater.* **8**, 074802 (2024).
- [62] S. Bötzsel, F. Lechermann, J. Gondolf, and I. M. Eremin, *Phys. Rev. B* **109**, L180502 (2024).
- [63] Z. Luo, B. Lv, M. Wang, W. Wú, and D.-X. Yao, *npj Quantum Materials* **9**, 61 (2024).
- [64] M. Kakoi, T. Kaneko, H. Sakakibara, M. Ochi, and K. Kuroki, *Phys. Rev. B* **109**, L201124 (2024).
- [65] S. Bötzsel, F. Lechermann, T. Shibauchi, and I. M. Eremin, *Communications Physics* **8**, 154 (2025).
- [66] W. Xi, S.-L. Yu, and J.-X. Li, *Phys. Rev. B* **111**, 104505 (2025).
- [67] J. Zhan, C. Le, X. Wu, and J. Hu, *Impact of nonlocal coulomb repulsion on superconductivity and density-wave orders in bilayer nickelates* (2025), arXiv:2503.18877 [cond-mat.supr-con].
- [68] C. Xia, H. Liu, S. Zhou, and H. Chen, *Nature Communications* **16**, 1054 (2025).
- [69] Z.-Y. Shao, Y.-B. Liu, M. Liu, and F. Yang, *Band structure and pairing nature of la₃ni₂O₇ thin film at ambient pressure* (2025), arXiv:2501.10409 [cond-mat.supr-con].
- [70] J.-B. de Vaulx, Q. N. Meier, P. Toulemonde, A. Cano, and V. Olevano, *Pressure and strain effects on the ab initio gw electronic structure of la₃ni₂O₇* (2025), arXiv:2504.21651 [cond-mat.supr-con].
- [71] F. Lechermann, S. Bötzsel, and I. M. Eremin, *Low-energy perspective of interacting electrons in the normal state of superconducting bilayer nickelate* (2025), arXiv:2503.12412 [cond-mat.str-el].
- [72] Y. Nomura, M. Kitatani, S. Sakai, and R. Arita, *Strong-coupling high-t_c superconductivity in doped correlated band insulator* (2025), arXiv:2502.14601 [cond-mat.supr-con].
- [73] T. A. Maier, P. Doak, L.-F. Lin, Y. Zhang, A. Moreo, and E. Dagotto, *Interlayer pairing in bilayer nickelates* (2025), arXiv:2506.07741 [cond-mat.str-el].
- [74] C. Yue, J.-J. Miao, H. Huang, Y. Hua, P. Li, Y. Li, G. Zhou, W. Lv, Q. Yang, H. Sun, Y.-J. Sun, J. Lin, Q.-K. Xue, Z. Chen, and W.-Q. Chen, *Correlated electronic structures and unconventional superconductivity in bilayer nickelate heterostructures* (2025), arXiv:2501.06875 [cond-mat.str-el].
- [75] C. Le, J. Zhan, X. Wu, and J. Hu, *Landscape of correlated orders in strained bilayer nickelate thin films* (2025), arXiv:2501.14665 [cond-mat.supr-con].
- [76] H. Li, X. Zhou, T. Nummy, J. Zhang, V. Pardo, W. E. Pickett, J. F. Mitchell, and D. S. Dessau, *Nature Communications* **8**, 704 (2017).
- [77] K. Momma and F. Izumi, *Journal of Applied Crystallography* **44**, 1272 (2011).
- [78] E. K. Ko, Y. Yu, Y. Liu, L. Bhatt, J. Li, V. Thamby, C.-T. Kuo, B. Y. Wang, Y. Lee, K. Lee, J.-S. Lee, B. H. Goodge, D. A. Muller, and H. Y. Hwang, *Nature* **638**, 935 (2025).
- [79] G. Zhou, W. Lv, H. Wang, Z. Nie, Y. Chen, Y. Li, H. Huang, W.-Q. Chen, Y.-J. Sun, Q.-K. Xue, and Z. Chen, *Nature* **640**, 641 (2025).
- [80] Y. Liu, E. K. Ko, Y. Tarn, L. Bhatt, J. Li, V. Thamby, B. H. Goodge, D. A. Muller, S. Raghu, Y. Yu, and H. Y. Hwang, *Nature Materials* **10**.1038/s41563-025-02258-y (2025).
- [81] Y.-F. Zhao and A. S. Botana, *Phys. Rev. B* **111**, 115154 (2025).
- [82] B. Geisler, J. J. Hamlin, G. R. Stewart, R. G. Hennig, and P. J.

- Hirschfeld, Electronic reconstruction and interface engineering of emergent spin fluctuations in compressively strained $\text{La}_3\text{Ni}_2\text{O}_7$ on $\text{SrLaAlO}_4(001)$ (2025), arXiv:2503.10902 [cond-mat.supr-con].
- [83] X.-W. Yi, W. Li, J.-Y. You, B. Gu, and G. Su, Unifying strain-driven and pressure-driven superconductivity in $\text{La}_3\text{Ni}_2\text{O}_7$: Suppressed charge/spin density waves and enhanced interlayer coupling (2025), arXiv:2505.12733 [cond-mat.supr-con].
- [84] P. Li, G. Zhou, W. Lv, Y. Li, C. Yue, H. Huang, L. Xu, J. Shen, Y. Miao, W. Song, Z. Nie, Y. Chen, H. Wang, W. Chen, Y. Huang, Z.-H. Chen, T. Qian, J. Lin, J. He, Y.-J. Sun, Z. Chen, and Q.-K. Xue, National Science Review , nwaf205 (2025).
- [85] B. Y. Wang, Y. Zhong, S. Abadi, Y. Liu, Y. Yu, X. Zhang, Y.-M. Wu, R. Wang, J. Li, Y. Tarn, E. K. Ko, V. Thampy, M. Hashimoto, D. Lu, Y. S. Lee, T. P. Devereaux, C. Jia, H. Y. Hwang, and Z.-X. Shen, Electronic structure of compressively strained thin film $\text{La}_2\text{Pr}\text{Ni}_2\text{O}_7$ (2025), arXiv:2504.16372 [cond-mat.supr-con].
- [86] L. Bhatt, A. Y. Jiang, E. K. Ko, N. Schnitzer, G. A. Pan, D. F. Segedin, Y. Liu, Y. Yu, Y.-F. Zhao, E. A. Morales, C. M. Brooks, A. S. Botana, H. Y. Hwang, J. A. Mundy, D. A. Muller, and B. H. Goodge, Resolving structural origins for superconductivity in strain-engineered $\text{La}_3\text{Ni}_2\text{O}_7$ thin films (2025), arXiv:2501.08204 [cond-mat.supr-con].
- [87] S. Fan, M. Ou, M. Scholten, Q. Li, Z. Shang, Y. Wang, J. Xu, H. Yang, I. M. Eremin, and H.-H. Wen, Superconducting gaps revealed by STM measurements on $\text{La}_2\text{Pr}\text{Ni}_2\text{O}_7$ thin films at ambient pressure (2025), arXiv:2506.01788 [cond-mat.supr-con].
- [88] B. Hao, M. Wang, W. Sun, Y. Yang, Z. Mao, S. Yan, H. Sun, H. Zhang, L. Han, Z. Gu, J. Zhou, D. Ji, and Y. Nie, Superconductivity and phase diagram in Sr-doped $\text{La}_{3-x}\text{Sr}_x\text{Ni}_2\text{O}_7$ thin films (2025), arXiv:2505.12603 [cond-mat.supr-con].
- [89] N. Marzari, A. A. Mostofi, J. R. Yates, I. Souza, and D. Vanderbilt, Rev. Mod. Phys. **84**, 1419 (2012).
- [90] J. P. Perdew, K. Burke, and M. Ernzerhof, Phys. Rev. Lett. **77**, 3865 (1996).
- [91] G. Kresse and J. Hafner, Phys. Rev. B **47**, 558–561 (1993).
- [92] G. Kresse and J. Furthmüller, Comput. Mater. Sci. **6**, 15 (1996).
- [93] G. Kresse and J. Furthmüller, Phys. Rev. B **54**, 11169–11186 (1996).
- [94] A. A. Mostofi, J. R. Yates, G. Pizzi, Y.-S. Lee, I. Souza, D. Vanderbilt, and N. Marzari, Computer Physics Communications **185**, 2309 (2014).
- [95] See Supplemental Material for additional data and discussion, which includes Refs. [66, 81, 86, 89–94, 96, 104–106].
- [96] N. E. Bickers, Self-consistent many-body theory for condensed matter systems, in Theoretical Methods for Strongly Correlated Electrons, edited by D. Sénéchal, A.-M. Tremblay, and C. Bourbonnais (Springer New York, New York, NY, 2004) pp. 237–296.
- [97] K. Ushio, S. Kamiyama, Y. Hoshi, R. Mizuno, M. Ochi, K. Kuroki, and H. Sakakibara, Theoretical study on ambient pressure superconductivity in $\text{La}_3\text{Ni}_2\text{O}_7$ thin films : structural analysis, model construction, and robustness of $s\pm$ -wave pairing (2025), arXiv:2506.20497 [cond-mat.supr-con].
- [98] K. Kuroki, T. Higashida, and R. Arita, Phys. Rev. B **72**, 212509 (2005).
- [99] P. J. Hirschfeld, M. M. Korshunov, and I. I. Mazin, Reports on Progress in Physics **74**, 124508 (2011).
- [100] X. Chen, S. Maiti, A. Linscheid, and P. J. Hirschfeld, Phys. Rev. B **92**, 224514 (2015).
- [101] A. Linscheid, S. Maiti, Y. Wang, S. Johnston, and P. J. Hirschfeld, Phys. Rev. Lett. **117**, 077003 (2016).
- [102] K. Matsumoto, D. Ogura, and K. Kuroki, Phys. Rev. B **97**, 014516 (2018).
- [103] M. Osada, C. Terakura, A. Kikkawa, M. Nakajima, H.-Y. Chen, Y. Nomura, Y. Tokura, and A. Tsukazaki, Communications Physics **8**, 251 (2025).
- [104] G. Rohringer, H. Hafermann, A. Toschi, A. Katanin, A. Antipov, M. Katsnelson, A. Lichtenstein, A. Rubtsov, and K. Held, Reviews of Modern Physics **90**, 025003 (2018), publisher: American Physical Society.
- [105] R. B. Lehoucq, D. C. Sorensen, and C. Yang, SIAM (1998).
- [106] J. Linder and A. V. Balatsky, Rev. Mod. Phys. **91**, 045005 (2019).

Supplemental Material for
“Optimal superconductivity near a Lifshitz transition in strained $(\text{La},\text{Pr})_3\text{Ni}_2\text{O}_7$ ”

Siheon Ryee,^{1,2,*} Niklas Witt,³ Giorgio Sangiovanni,³ and Tim O. Wehling^{1,2}

¹*Institute of Theoretical Physics, University of Hamburg, Notkestraße 9-11, 22607 Hamburg, Germany*

²*The Hamburg Centre for Ultrafast Imaging, Luruper Chaussee 149, 22761 Hamburg, Germany*

³*Institut für Theoretische Physik und Astrophysik and Würzburg-Dresden Cluster
of Excellence ct.qmat, Universität Würzburg, 97074 Würzburg, Germany*

CONTENTS

SM1. Model construction for strained bilayer nickelates	S2
SM2. Pairing interactions and the gap equation	S3
A. Pairing interactions	S3
B. Solving the gap equation	S4
SM3. Derivation of Eq. (5) in the main text	S5
A. Basis transformation	S5
B. Eq. (5) in the main text	S5
SM4. Influence of Hund’s coupling and interlayer interactions	S6
SM5. Additional data: Gap function on the Fermi surface	S7
SM6. Additional data: Doping dependence	S7
References	S8

* suheon.ryee@uni-hamburg.de

SM1. MODEL CONSTRUCTION FOR STRAINED BILAYER NICKELATES

We first performed DFT calculations using the Vienna Ab initio Simulation Package (VASP) [S1–S3] using DFT-optimized lattice constants of strained $\text{La}_3\text{Ni}_2\text{O}_7$ reported in Ref. [S4]. In Ref. [S4], the in-plane (a and b) and out-of-plane (c) lattice constants of the experimentally relevant Fmmm structure [S5] are reported for strains of -3 % and 3 %. Noting that the DFT-optimized lattice constants of the Amam structure vary nearly linearly with strain [S4], we performed a linear interpolation of the Fmmm lattice constants between -3 % and 3 % to estimate the values at intermediate strains. Since the in-plane lattice constants a and b only differ by about 1 % in the orthorhombic Fmmm structure [S4, S5], we use higher-symmetry tetragonal I4/mmm structure by averaging a and b . Atomic positions were relaxed until the force was smaller than 1 meV/Å. We used $7 \times 7 \times 7$ and $15 \times 15 \times 15$ momentum grids for the atomic relaxation and electronic structure calculations, respectively, for the primitive unit cell at each strain. We employed the Perdew–Burke–Ernzerhof (PBE) parametrization of the generalized gradient approximation for the exchange-correlation functional [S6] as in Ref. [S4] and the plane-wave energy cutoff of 500 eV.

TABLE S1. Hopping amplitudes in units of eV.

	Strain									
	-3 %	-2.5 %	-2.25 %	-2 %	-1.5 %	-1 %	0 %	1 %	2 %	3 %
ϵ_0	0.7306	0.6467	0.6045	0.5556	0.4963	0.4308	0.3049	0.1891	0.0856	-0.0105
t_1^x	-0.4999	-0.4925	-0.4884	-0.4829	-0.4756	-0.4666	-0.4486	-0.4313	-0.4148	-0.3986
t_2^x	0.0727	0.0714	0.0708	0.0700	0.0690	0.0677	0.0656	0.0637	0.0617	0.0594
t_3^x	-0.0544	-0.0524	-0.0514	-0.0501	-0.0489	-0.0477	-0.0455	-0.0430	-0.0405	-0.0385
t_1^z	-0.0825	-0.0870	-0.0892	-0.0914	-0.0947	-0.0998	-0.1085	-0.1162	-0.1232	-0.1306
t_2^z	-0.0142	-0.0141	-0.0142	-0.0143	-0.0148	-0.0158	-0.0174	-0.0184	-0.0194	-0.0206
t_{\perp}^x	-0.0021	-0.0023	-0.0023	-0.0025	-0.0029	-0.0036	-0.0052	-0.0062	-0.0073	-0.0085
$t_{\perp,1}^x$	-0.0036	-0.0035	-0.0033	-0.0031	-0.0031	-0.0032	-0.0031	-0.0030	-0.0030	-0.0031
$t_{\perp,2}^x$	0.0018	0.0019	0.0019	0.0020	0.0021	0.0023	0.0027	0.0030	0.0031	0.0033
t_{\perp}^z	-0.6408	-0.6424	-0.6418	-0.6406	-0.6380	-0.6265	-0.6048	-0.5909	-0.5832	-0.5752
$t_{\perp,1}^z$	0.0049	0.0074	0.0087	0.0102	0.0126	0.0165	0.0235	0.0283	0.0316	0.0343
$t_{\perp,2}^z$	0.0080	0.0086	0.0086	0.0088	0.0088	0.0084	0.0077	0.0072	0.0073	0.0072
t_1^{xz}	0.2084	0.2103	0.2113	0.2124	0.2145	0.2178	0.2227	0.2253	0.2273	0.2292
t_3^{xz}	0.0242	0.0235	0.0232	0.0228	0.0226	0.0226	0.0224	0.0221	0.0216	0.0213
$t_{\perp,1}^{xz}$	-0.0276	-0.0286	-0.0291	-0.0291	-0.0295	-0.0302	-0.0307	-0.0309	-0.0311	-0.0313

We then used the Wannier90 code [S7] to construct a four-orbital (top-layer two Ni- e_g + bottom-layer two Ni- e_g) bilayer square-lattice model of strained $\text{La}_3\text{Ni}_2\text{O}_7$ using the maximally localized Wannier function (MLWF) method [S8]. We hereafter denote the $d_{x^2-y^2}$ orbital by x and the d_{z^2} orbital by z for brevity. The resulting four-orbital tight-binding Hamiltonian H_0 on the bilayer square lattice reads

$$H_0 = \sum_{\mathbf{k}\sigma} \Psi_{\mathbf{k}\sigma}^\dagger \mathbf{h}(\mathbf{k}) \Psi_{\mathbf{k}\sigma}, \quad (\text{S1})$$

where $\Psi_{\mathbf{k}\sigma} = [d_{\mathbf{k}\bar{x}\sigma}, d_{\mathbf{k}\bar{z}\sigma}, d_{\mathbf{k}x\sigma}, d_{\mathbf{k}z\sigma}]^T$ with $\bar{\eta}$ and $\underline{\eta}$ ($\eta \in \{x, z\}$) referring to the orbital in the top and bottom layers, respectively. d denotes the corresponding electron annihilation operator. σ denotes spin and \mathbf{k} the crystal momentum in the first Brillouin zone. $\mathbf{h}(\mathbf{k})$ reads

$$\mathbf{h}(\mathbf{k}) = \begin{pmatrix} h_{11}(\mathbf{k}) & h_{12}(\mathbf{k}) & h_{13}(\mathbf{k}) & h_{14}(\mathbf{k}) \\ h_{12}(\mathbf{k}) & h_{22}(\mathbf{k}) & h_{23}(\mathbf{k}) & h_{24}(\mathbf{k}) \\ h_{13}(\mathbf{k}) & h_{23}(\mathbf{k}) & h_{33}(\mathbf{k}) & h_{34}(\mathbf{k}) \\ h_{14}(\mathbf{k}) & h_{24}(\mathbf{k}) & h_{34}(\mathbf{k}) & h_{44}(\mathbf{k}) \end{pmatrix} \quad (\text{S2})$$

where the matrix elements of $\mathbf{h}(\mathbf{k})$ are given by

$$\begin{aligned}
h_{11}(\mathbf{k}) &= h_{33}(\mathbf{k}) = \frac{\epsilon_0}{2} + 2t_1^x(\cos k_x + \cos k_y) + 4t_2^x \cos k_x \cos k_y + 2t_3^x(\cos 2k_x + \cos 2k_y), \\
h_{22}(\mathbf{k}) &= h_{44}(\mathbf{k}) = -\frac{\epsilon_0}{2} + 2t_1^z(\cos k_x + \cos k_y) + 4t_2^z \cos k_x \cos k_y, \\
h_{12}(\mathbf{k}) &= 2t_1^{xz}(\cos k_x - \cos k_y) + 2t_3^{xz}(\cos 2k_x - \cos 2k_y), \\
h_{13}(\mathbf{k}) &= t_{\perp}^x + 2t_{\perp,1}^x(\cos k_x + \cos k_y) + 4t_{\perp,2}^x \cos k_x \cos k_y, \\
h_{14}(\mathbf{k}) &= 2t_{\perp,1}^{xz}(\cos k_x - \cos k_y), \\
h_{24}(\mathbf{k}) &= t_{\perp}^z + 2t_{\perp,1}^z(\cos k_x + \cos k_y) + 4t_{\perp,2}^z \cos k_x \cos k_y, \\
h_{23}(\mathbf{k}) &= h_{14}(\mathbf{k}), \\
h_{34}(\mathbf{k}) &= h_{12}(\mathbf{k}).
\end{aligned} \tag{S3}$$

The hopping amplitudes are listed in Table S1.

SM2. PAIRING INTERACTIONS AND THE GAP EQUATION

A. Pairing interactions

We consider the following interaction Hamiltonian H_{int} for the bilayer e_g manifold:

$$\begin{aligned}
H_{\text{int}} = U \sum_{\eta} (n_{\bar{\eta}\uparrow} n_{\bar{\eta}\downarrow} + n_{\underline{\eta}\uparrow} n_{\underline{\eta}\downarrow}) + \sum_{\substack{\eta < \eta' \\ \sigma, \sigma'}} (U' - J \delta_{\sigma\sigma'}) (n_{\bar{\eta}\sigma} n_{\bar{\eta}'\sigma'} + n_{\underline{\eta}\sigma} n_{\underline{\eta}'\sigma'}) \\
+ J \sum_{\eta \neq \eta'} \left(d_{\bar{\eta}\uparrow}^\dagger d_{\bar{\eta}'\downarrow}^\dagger d_{\bar{\eta}\downarrow} d_{\bar{\eta}'\uparrow} + d_{\bar{\eta}\uparrow}^\dagger d_{\bar{\eta}'\downarrow}^\dagger d_{\bar{\eta}'\downarrow} d_{\bar{\eta}'\uparrow} + d_{\underline{\eta}\uparrow}^\dagger d_{\underline{\eta}'\downarrow}^\dagger d_{\underline{\eta}\downarrow} d_{\underline{\eta}'\uparrow} + d_{\underline{\eta}\uparrow}^\dagger d_{\underline{\eta}'\downarrow}^\dagger d_{\underline{\eta}'\downarrow} d_{\underline{\eta}'\uparrow} \right) \\
+ V \sum_{\substack{\eta, \eta' \\ \sigma, \sigma'}} n_{\bar{\eta}\sigma} n_{\eta'\sigma'}
\end{aligned} \tag{S4}$$

where $\eta, \eta' \in \{x, z\}$ and $\sigma, \sigma' \in \{\uparrow, \downarrow\}$. $\bar{\eta}$ and $\underline{\eta}$ denote the orbital in the top and bottom layers, respectively. $n_{\eta\sigma} = d_{\eta\sigma}^\dagger d_{\eta\sigma}$ is the corresponding electron number operator. The first three terms constitute the Kanamori-type local interaction Hamiltonian which includes intraorbital onsite Coulomb repulsion U , Hund's coupling J , and the interorbital onsite Coulomb repulsion $U' = U - 2J$. The last term, including the interlayer density-density interaction V , accounts for nonlocal interlayer interaction between the e_g orbitals in the top and bottom layers within the same cell. Equation (S4) can be recast as

$$H_{\text{int}} = \frac{1}{2} \sum_{i, l_1 l_2 l_3 l_4, \sigma\sigma'} \mathcal{U}_{l_1 l_4 l_3 l_2}^{\sigma\sigma'} d_{il_1\sigma}^\dagger d_{il_2\sigma'}^\dagger d_{il_3\sigma'} d_{il_4\sigma}, \tag{S5}$$

where $l_i \in \{\bar{x}, \bar{z}, x, z\}$. Furthermore, $U \equiv \mathcal{U}_{\bar{l}\bar{l}\bar{l}\bar{l}}^{\sigma\sigma} = \mathcal{U}_{\bar{l}\bar{l}\bar{l}\bar{l}}^{\sigma-\sigma} = \mathcal{U}_{\underline{l}\underline{l}\underline{l}\underline{l}}^{\sigma\sigma} = \mathcal{U}_{\underline{l}\underline{l}\underline{l}\underline{l}}^{\sigma-\sigma}$, $U' \equiv \mathcal{U}_{\bar{l}\bar{l}'\bar{l}'\bar{l}'}^{\sigma\sigma} = \mathcal{U}_{\bar{l}\bar{l}'\bar{l}'\bar{l}'}^{\sigma-\sigma} = \mathcal{U}_{\underline{l}'\underline{l}'\underline{l}'\underline{l}'}^{\sigma\sigma} = \mathcal{U}_{\underline{l}'\underline{l}'\underline{l}'\underline{l}'}^{\sigma-\sigma}$, and $J \equiv \mathcal{U}_{\bar{l}\bar{l}'\bar{l}'}^{\sigma\sigma} = \mathcal{U}_{\bar{l}\bar{l}'\bar{l}'}^{\sigma-\sigma} = \mathcal{U}_{\bar{l}'\bar{l}\bar{l}'}^{\sigma\sigma} = \mathcal{U}_{\bar{l}'\bar{l}\bar{l}'}^{\sigma-\sigma} = \mathcal{U}_{\underline{l}'\underline{l}'\underline{l}'}^{\sigma\sigma} = \mathcal{U}_{\underline{l}'\underline{l}'\underline{l}'}^{\sigma-\sigma}$ with $l \neq l'$. Lastly, $V \equiv \mathcal{U}_{\bar{l}\bar{l}'\bar{l}'}^{\sigma\sigma} = \mathcal{U}_{\bar{l}\bar{l}'\bar{l}'}^{\sigma-\sigma} = \mathcal{U}_{\underline{l}'\underline{l}'\underline{l}'}^{\sigma\sigma} = \mathcal{U}_{\underline{l}'\underline{l}'\underline{l}'}^{\sigma-\sigma}$ where either $l \neq l'$ or $l = l'$.

From Eq. (S5), elements of the spin (sp) and charge (ch) channel vertices $\Gamma^{\text{sp/ch}}$ within the random phase approximation (RPA) are given by [S9]

$$\Gamma_{l_1 l_2 l_3 l_4}^{\text{sp/ch}} = \mathcal{U}_{l_1 l_2 l_3 l_4}^{\uparrow\downarrow} \mp (\mathcal{U}_{l_1 l_2 l_3 l_4}^{\uparrow\uparrow} - \mathcal{U}_{l_1 l_3 l_2 l_4}^{\uparrow\uparrow}), \tag{S6}$$

where the terms in parentheses ensure the antisymmetrization of the Coulomb vertex. In the e_g -orbital basis, elements of $\Gamma^{\text{sp/ch}}$ read

$$\Gamma_{\bar{\eta}_1 \bar{\eta}_2 \bar{\eta}_3 \bar{\eta}_4}^{\text{sp}} = \Gamma_{\underline{\eta}_1 \underline{\eta}_2 \underline{\eta}_3 \underline{\eta}_4}^{\text{sp}} = \begin{cases} U & \text{if } \eta_1 = \eta_2 = \eta_3 = \eta_4, \\ U' & \text{if } \eta_1 = \eta_3 \neq \eta_2 = \eta_4, \\ J & \text{if } \eta_1 = \eta_2 \neq \eta_3 = \eta_4, \\ J & \text{if } \eta_1 = \eta_4 \neq \eta_2 = \eta_3, \end{cases} \quad \Gamma_{\bar{\eta}_1 \bar{\eta}_2 \bar{\eta}_3 \bar{\eta}_4}^{\text{ch}} = \Gamma_{\underline{\eta}_1 \underline{\eta}_2 \underline{\eta}_3 \underline{\eta}_4}^{\text{ch}} = \begin{cases} U & \text{if } \eta_1 = \eta_2 = \eta_3 = \eta_4, \\ -U' + 2J & \text{if } \eta_1 = \eta_3 \neq \eta_2 = \eta_4, \\ 2U' - J & \text{if } \eta_1 = \eta_2 \neq \eta_3 = \eta_4, \\ J & \text{if } \eta_1 = \eta_4 \neq \eta_2 = \eta_3, \end{cases} \tag{S7}$$

and

$$\Gamma_{\bar{\eta}\underline{\eta}'\bar{\eta}\underline{\eta}'}^{\text{sp}} = \Gamma_{\underline{\eta}\bar{\eta}'\underline{\eta}\eta'}^{\text{sp}} = V, \quad \Gamma_{\bar{\eta}\underline{\eta}'\bar{\eta}\underline{\eta}'}^{\text{ch}} = \Gamma_{\underline{\eta}\bar{\eta}'\underline{\eta}\eta'}^{\text{ch}} = -V, \quad \Gamma_{\bar{\eta}\bar{\eta}'\underline{\eta}'\eta'}^{\text{ch}} = \Gamma_{\underline{\eta}\eta'\bar{\eta}'\eta'}^{\text{ch}} = 2V, \quad (\text{S8})$$

where either $\eta = \eta'$ or $\eta \neq \eta'$. The other remaining elements are zero. The spin and charge susceptibilities are obtained using these vertices from the Bethe-Salpeter equation as

$$\chi_{l_1 l_2 l_7 l_8}^{\text{sp/ch}}(q) = \chi_{l_1 l_2 l_7 l_8}^0(q) \pm \chi_{l_1 l_2 l_3 l_4}^{\text{sp/ch}}(q) \Gamma_{l_3 l_4 l_5 l_6}^{\text{sp/ch}} \chi_{l_5 l_6 l_7 l_8}^0(q), \quad (\text{S9})$$

$$= [\chi^0(q) [1 \mp \Gamma^{\text{sp/ch}} \chi^0(q)]^{-1}]_{l_1 l_2 l_7 l_8}, \quad (\text{S10})$$

where $\chi_{l_1 l_2 l_3 l_4}^0(q) = -\frac{T}{N} \sum_{\mathbf{k}} G_{l_2 l_3}(k+q) G_{l_4 l_2}(k)$. $k \equiv (\mathbf{k}, i\omega_n)$ and $q \equiv (\mathbf{q}, i\nu_n)$ with \mathbf{k} and \mathbf{q} being the crystal momentum and ω_n (ν_n) the fermionic (bosonic) Matsubara frequency. T is temperature, N the number of \mathbf{k} points in the first Brillouin zone, and $G(k)$ the Green's function. Here, indices repeated twice should be summed over. By employing the parquet equations [S9, S10] and using $\Gamma^{\text{sp/ch}}$ and $\chi^{\text{sp/ch}}$, one can express the effective RPA singlet (s) and triplet (t) pairing interactions appearing in Eq. (1) in the main text as

$$\Gamma_{l_1 l_4 l_3 l_2}^{\text{s}}(q) = \frac{3}{2} \Gamma_{l_1 l_4 l_3 l_2}^{\text{sp}} + \frac{1}{2} \Gamma_{l_1 l_4 l_3 l_2}^{\text{ch}} + 3[\Gamma^{\text{sp}} \chi^{\text{sp}}(q) \Gamma^{\text{sp}}]_{l_1 l_4 l_3 l_2} - [\Gamma^{\text{ch}} \chi^{\text{ch}}(q) \Gamma^{\text{ch}}]_{l_1 l_4 l_3 l_2}, \quad (\text{S11})$$

$$\Gamma_{l_1 l_4 l_3 l_2}^{\text{t}}(q) = -\frac{1}{2} \Gamma_{l_1 l_4 l_3 l_2}^{\text{sp}} + \frac{1}{2} \Gamma_{l_1 l_4 l_3 l_2}^{\text{ch}} - [\Gamma^{\text{sp}} \chi^{\text{sp}}(q) \Gamma^{\text{sp}}]_{l_1 l_4 l_3 l_2} - [\Gamma^{\text{ch}} \chi^{\text{ch}}(q) \Gamma^{\text{ch}}]_{l_1 l_4 l_3 l_2}. \quad (\text{S12})$$

B. Solving the gap equation

The transition to a superconducting phase is indicated by the divergence of the corresponding pairing susceptibility. Using the above formulas, it can be formulated in terms of a non-Hermitian eigenvalue problem in the normal state, namely the gap equation [Eq. (1) in the main text] [S9], which reads

$$\lambda_{\text{sc}} \Delta_{l_1 l_2}(k) = -\frac{T}{2N} \sum_{q, l_1 l_2 l_3 l_4} \Gamma_{l_1 l_4 l_3 l_2}^{s/\text{t}}(q) G_{l_4 l_5}(k-q) G_{l_3 l_6}(q-k) \Delta_{l_5 l_6}(k-q), \quad (\text{S13})$$

where λ_{sc} is the eigenvalue and $\Delta_{l_1 l_2}(k)$ the gap function. We investigate the leading λ_{sc} at a fixed $T = 1/140$ eV $\simeq 83$ K using 140×140 momentum (\mathbf{k} and \mathbf{q}) grids in the first Brillouin zone.

We employed the implicitly restarted Arnoldi method using the ARPACK library [S11] to compute the leading eigenvalue and the associated gap function of Eq. (S13). We set a cutoff energy $\omega_{\text{cut}} = 8$ eV for the fermionic Matsubara frequency in $\Delta(\mathbf{k}, i\omega)$ to ensure that the matrix size in the gap equation remains numerically tractable without losing accuracy. As a result, $\Delta(\mathbf{k}, i\omega)$ is defined only within the frequency range of $[-\omega_{\text{cut}}, \omega_{\text{cut}}]$. λ_{sc} is found to be nearly converged at $\omega_{\text{cut}} \simeq 2$ eV (see Fig. S1), suggesting that $\Delta(\mathbf{k}, i\omega)$ has significant magnitude only within the Matsubara frequency range of approximately $[-2, 2]$ eV and decays rapidly with increasing $|i\omega|$.

The gap functions must satisfy the following transformation properties under the exchange of spin (\hat{S}), parity (\hat{P}), orbital (\hat{O}), and time (\hat{T}) [S12]:

$$\hat{S} \Delta_{l_1 l_2}(\mathbf{k}, i\omega) = \pm \Delta_{l_1 l_2}(\mathbf{k}, i\omega), \quad (+ \text{ for triplet, } - \text{ for singlet}) \quad (\text{S14})$$

$$\hat{P} \Delta_{l_1 l_2}(\mathbf{k}, i\omega) = \pm \Delta_{l_1 l_2}(-\mathbf{k}, i\omega), \quad (\text{S15})$$

$$\hat{O} \Delta_{l_1 l_2}(\mathbf{k}, i\omega) = \pm \Delta_{l_2 l_1}(\mathbf{k}, i\omega), \quad (\text{S16})$$

$$\hat{T} \Delta_{l_1 l_2}(\mathbf{k}, i\omega) = \pm \Delta_{l_1 l_2}(\mathbf{k}, -i\omega). \quad (\text{S17})$$

The anti-symmetry of the gap function, dictated by the Pauli principle, leads to the constraint:

$$\hat{S} \hat{P} \hat{O} \hat{T} \Delta_{l_1 l_2}(\mathbf{k}, i\omega) = -\Delta_{l_1 l_2}(\mathbf{k}, i\omega). \quad (\text{S18})$$

We explored all possible symmetries consistent with the above “SPOT” condition when solving Eq. (S13). Note that the s_{\pm} -wave and $d_{x^2-y^2}$ -wave gap functions are both odd under \hat{S} (i.e., singlet), and even under \hat{P} , \hat{O} , and \hat{T} , while they belong to different irreducible representations (A_{1g} for the s_{\pm} wave and B_{1g} for the $d_{x^2-y^2}$ wave).

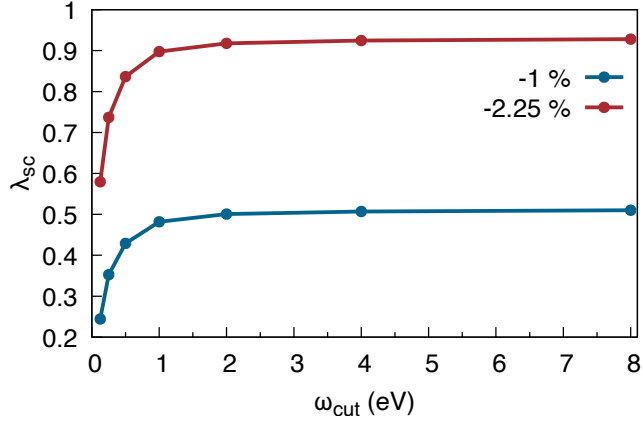


FIG. S1. The calculated leading eigenvalue λ_{sc} at -1% and -2.25% strains as a function of the cutoff energy ω_{cut} for the fermionic Matsubara frequency in $\Delta(\mathbf{k}, i\omega)$. $U = 0.96$ eV, $J = U/6$ and $V = 0$.

SM3. DERIVATION OF EQ. (5) IN THE MAIN TEXT

A. Basis transformation

The bonding-antibonding (BA) orbital basis in which the electron annihilation operator d_{l_\pm} (site and spin indices are omitted for simplicity) is defined as the symmetric (+) and antisymmetric (−) combinations of the top and bottom layer e_g orbital operators:

$$\begin{pmatrix} d_{x_+} \\ d_{z_+} \\ d_{x_-} \\ d_{z_-} \end{pmatrix} = \frac{1}{\sqrt{2}} \begin{pmatrix} 1 & 0 & 1 & 0 \\ 0 & 1 & 0 & 1 \\ 1 & 0 & -1 & 0 \\ 0 & 1 & 0 & -1 \end{pmatrix} \begin{pmatrix} d_{\bar{x}} \\ d_{\bar{z}} \\ d_{\underline{x}} \\ d_{\underline{z}} \end{pmatrix} = \mathbf{A} \begin{pmatrix} d_{\bar{x}} \\ d_{\bar{z}} \\ d_{\underline{x}} \\ d_{\underline{z}} \end{pmatrix}, \text{ where } \mathbf{A} \equiv \frac{1}{\sqrt{2}} \begin{pmatrix} 1 & 0 & 1 & 0 \\ 0 & 1 & 0 & 1 \\ 1 & 0 & -1 & 0 \\ 0 & 1 & 0 & -1 \end{pmatrix}. \quad (\text{S19})$$

Note that $\mathbf{A}^{-1} = \mathbf{A}$. Under this basis transformation, the vertices Γ^r (with $r = s, t, sp, ch$) and susceptibilities χ^r (with $r = 0, sp, ch$) are transformed into the BA basis as

$$\Gamma_{ijkl}^r(q) = \sum_{abcd} A_{ia} A_{jb} A_{kc} A_{ld} \Gamma_{abcd}^r(q), \quad \chi_{ijkl}^r(q) = \sum_{abcd} A_{ia} A_{jb} A_{kc} A_{ld} \chi_{abcd}^r(q), \quad (\text{S20})$$

where $i, j, k, l \in \{x_+, z_+, x_-, z_-\}$ and $a, b, c, d \in \{\bar{x}, \bar{z}, \underline{x}, \underline{z}\}$.

B. Eq. (5) in the main text

We now investigate which irreducible susceptibility governs the relevant singlet pairing interactions. The charge susceptibility χ^{ch} is found to be much smaller than the spin susceptibility χ^{sp} , so terms containing χ^{ch} can be neglected for our purpose. Expanding the spin susceptibility χ^{sp} in terms of the irreducible (bubble) susceptibility $\chi^0(q)$, we can express Eq. (S11) as

$$\begin{aligned} \Gamma^s(q) &\simeq \frac{3}{2} \Gamma^{sp} + \frac{1}{2} \Gamma^{ch} + 3\Gamma^{sp} \chi^{sp}(q) \Gamma^{sp} \\ &= \frac{3}{2} \Gamma^{sp} + \frac{1}{2} \Gamma^{ch} + 3\Gamma^{sp} [\chi^0(q) + \chi^0(q) \Gamma^{sp} \chi^0(q) + \chi^0(q) \Gamma^{sp} \chi^0(q) \Gamma^{sp} \chi^0(q) + \dots] \Gamma^{sp}. \end{aligned} \quad (\text{S21})$$

Retaining terms up to second order in interactions, this expression reduces to

$$\Gamma^s(q) \simeq \frac{3}{2} \Gamma^{sp} + \frac{1}{2} \Gamma^{ch} + 3\Gamma^{sp} \chi^0(q) \Gamma^{sp}. \quad (\text{S22})$$

We are interested in $\Gamma_{z_+z_+z_+z_+}^s$, $\Gamma_{z_-z_-z_-z_-}^s$, $\Gamma_{z_+z_-z_-z_+}^s$, and $\Gamma_{z_-z_+z_+z_-}^s$ appearing in Eq. (4) in the main text. Using Eqs. (S20) and (S22), and neglecting second order terms containing J since $J \ll U$, we can express them as

$$\begin{aligned}\Gamma_{z_+z_+z_+z_+}^s(q) &\simeq U + \frac{3}{4}V + \frac{3}{4}(U + V)^2\chi_{z_+z_+z_+z_+}^0(q) + \frac{3}{4}(U - V)^2\chi_{z_-z_-z_-z_-}^0(q) \\ &\simeq U + \frac{3}{4}V + \frac{3}{4}(U + V)^2\chi_{z_+z_+z_+z_+}^0(q), \\ \Gamma_{z_-z_-z_-z_-}^s(q) &\simeq U + \frac{3}{4}V + \frac{3}{4}(U + V)^2\chi_{z_-z_-z_-z_-}^0(q) + \frac{3}{4}(U - V)^2\chi_{z_+z_+z_+z_-}^0(q) \\ &\simeq U + \frac{3}{4}V + \frac{3}{4}(U - V)^2\chi_{z_+z_+z_+z_-}^0(q), \\ \Gamma_{z_+z_-z_-z_+}^s(q) &= \Gamma_{z_-z_+z_+z_-}^s(q) \simeq U + \frac{3}{4}V + \frac{3}{4}(U^2 - V^2)[\chi_{z_+z_-z_+z_-}^0(q) + \chi_{z_-z_+z_+z_-}^0(q)] \\ &= U + \frac{3}{4}V + \frac{3}{2}(U^2 - V^2)\chi_{z_+z_-z_+z_-}^0(q),\end{aligned}\tag{S23}$$

where we have omitted the term containing $\chi_{z_-z_-z_-z_-}^0(q)$ since $\chi_{z_-z_-z_-z_-}^0(q) \ll \chi_{z_+z_+z_+z_+}^0(q)$. Although it is strictly valid for strains $> -2.5\%$ [cf. Fig. S2], neglecting $\chi_{z_-z_-z_-z_-}^0(q)$ over the entire strain range does not affect our discussion. We used the identity $\chi_{z_+z_-z_+z_-}^0(q) = \chi_{z_-z_+z_-z_+}^0(q)$. In the case where $V = 0$, the above Eq. (S23) reduces to

$$\begin{aligned}\Gamma_{z_+z_+z_+z_+}^s(q) &= \Gamma_{z_-z_-z_-z_-}^s(q) \simeq U + \frac{3}{4}U^2\chi_{z_+z_+z_+z_+}^0(q), \\ \Gamma_{z_+z_-z_-z_+}^s(q) &= \Gamma_{z_-z_+z_+z_-}^s(q) \simeq U + \frac{3}{2}U^2\chi_{z_+z_-z_+z_-}^0(q),\end{aligned}\tag{S24}$$

which corresponds to Eq. (5) in the main text.

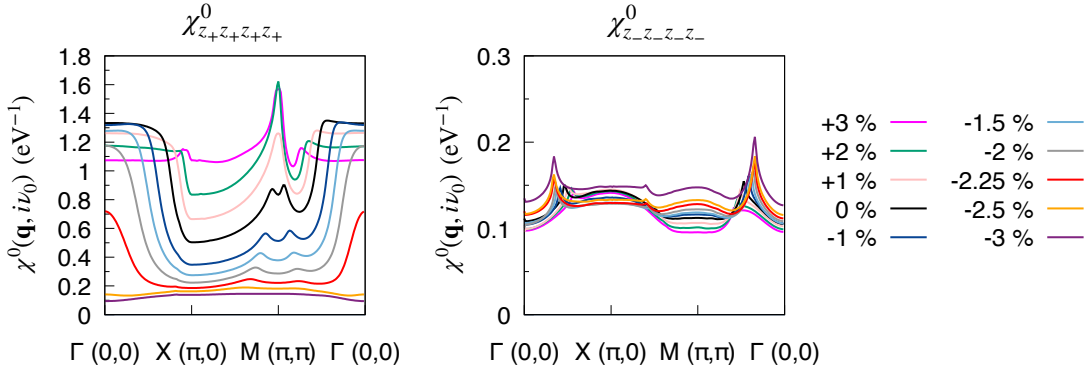


FIG. S2. The irreducible susceptibilities $\chi_{z_+z_+z_+z_+}^0(\mathbf{q}, iv_0)$ (left) and $\chi_{z_-z_-z_-z_-}^0(\mathbf{q}, iv_0)$ (right), at the lowest bosonic Matsubara frequency $v_0 = 0$, presented over the entire strain range.

SM4. INFLUENCE OF HUND'S COUPLING AND INTERLAYER INTERACTIONS

Figure S3 illustrates the dependence of the leading superconducting eigenvalue λ_{sc} on (a) Hund's coupling J and (b) the interlayer density-density interaction V .

The influence of J is found to be minor within a physically reasonable range. On the tensile strain side, increasing J promotes $d_{x^2-y^2}$ -wave pairing as the leading instability. In contrast, on the compressive strain side, the leading pairing instability is always the s_{\pm} -wave gap.

The effect of V differs between the compressive and tensile strain regimes: while λ_{sc} decreases with increasing V under compressive strain, it tends to increase at zero strain and under tensile strain. This behavior arises because V enhances $\Gamma_{z_+z_+z_+z_+}^s$, which acts as a pair-breaking interaction for the s_{\pm} -wave pairing (compressive strain side), but as a pair-forming interaction for the $d_{x^2-y^2}$ -wave pairing (tensile strain side). This can be understood from recalling Eq. (S23) which reads

$$\Gamma_{z_+z_+z_+z_+}^s(q) \simeq U + \frac{3}{4}V + \frac{3}{4}(U + V)^2\chi_{z_+z_+z_+z_+}^0(q).\tag{S25}$$

Thus, $\Gamma_{z_+z_+z_+z_+}^s(q)$ increases with V , and the contribution from the irreducible susceptibility $\chi_{z_+z_+z_+z_+}^0(q)$ becomes more significant as V grows. As shown in Fig. S2(a), $\chi_{z_+z_+z_+z_+}^0(q)$ develops a peak at the M point (π, π) of the FBZ on the tensile strain sides. For the $d_{x^2-y^2}$ -wave pairing symmetry [see the inset of Fig. S3(a)], this momentum $q = (\pi, \pi)$ connects two regions of the dominant gap component $\Delta_{z_+z_+}$ that have opposite signs. Consequently, the associated fluctuation $\chi_{z_+z_+z_+z_+}^0$ and the resulting $\Gamma_{z_+z_+z_+z_+}^s$ acts as a pair-forming channel for the $d_{x^2-y^2}$ -wave pairing.

This behavior—namely, the suppression of s_{\pm} -wave pairing and the enhancement of $d_{x^2-y^2}$ -wave pairing with increasing V is consistent with a recent study using the fluctuation-exchange approximation [S13].

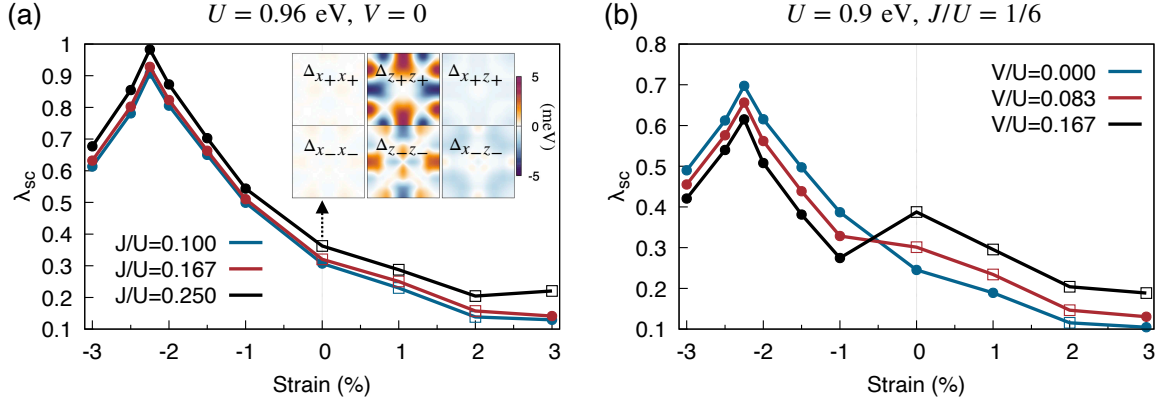


FIG. S3. (a) The leading λ_{sc} as a function of strain (bottom) for different values of J/U at $U = 0.96$ eV and $V = 0$. The inset shows the nonzero elements of the $d_{x^2-y^2}$ -wave gap function $\Delta_{lm}(k, i\omega_0)$ in the BA basis at 0 % strain. (b) The leading λ_{sc} as a function of strain (bottom) for different values of V/U at $U = 0.9$ eV and $J = U/6 \approx 0.167U$. Circles: s_{\pm} -wave gap; squares: $d_{x^2-y^2}$ -wave gap.

SM5. ADDITIONAL DATA: GAP FUNCTION ON THE FERMI SURFACE

Figure S4 shows the gap function on the band n closest to the Fermi level, $\hat{\Delta}_n(k, i\omega_0)$ ($\omega_0 = \pi T$ is the lowest fermionic Matsubara frequency). It is obtained by projecting the gap function $\Delta_{l_1 l_2}(k, i\omega_0)$ in the e_g -basis onto the band n closest to the Fermi level at each momentum k : $\hat{\Delta}_n(k, i\omega_0) = \sum_{l_1 l_2} P_{nl_1}^{-1} \Delta_{l_1 l_2}(k, i\omega_0) P_{l_2 n}$ where $P_{nl_1}^{-1}$ and $P_{l_2 n}$ are elements of the basis transformation matrices from the e_g orbitals l_1 and l_2 to the band n , respectively.

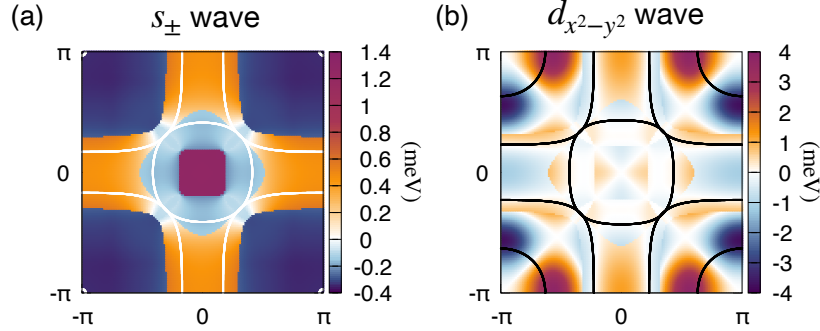


FIG. S4. (a) The s_{\pm} -wave gap at $U = 0.96$ eV, $J = U/6$, and $V = 0$ for -2.25% strain. (a) The $d_{x^2-y^2}$ -wave gap at $U = 0.9$ eV and $J = V = U/6$ for 0% strain. The white solid lines in (a) and black solid lines in (b) indicate the corresponding FSS.

SM6. ADDITIONAL DATA: DOPING DEPENDENCE

Figure S5 shows the variation of the leading eigenvalue λ_{sc} as a function of doping x , where $x < 0$ corresponds to electron doping and $x > 0$ to hole doping. Notably, λ_{sc} reaches its maximum when the γ pocket is marginally present in the Fermi surface for both -2.5% and -1.5% strains [Fig. S5(a)]. A closer inspection reveals that this behavior originates from a delicate balance

between the pair-breaking channel ($\chi_{z_+z_+z_+z_+}^0$) and the pair-forming channel ($\chi_{z_-z_-z_-z_-}^0$), both of which are promoted by the presence of the γ pocket [Figs. S5(b,c)]. This interplay is analogous to what we have observed in the strain-dependent analysis throughout the main text.

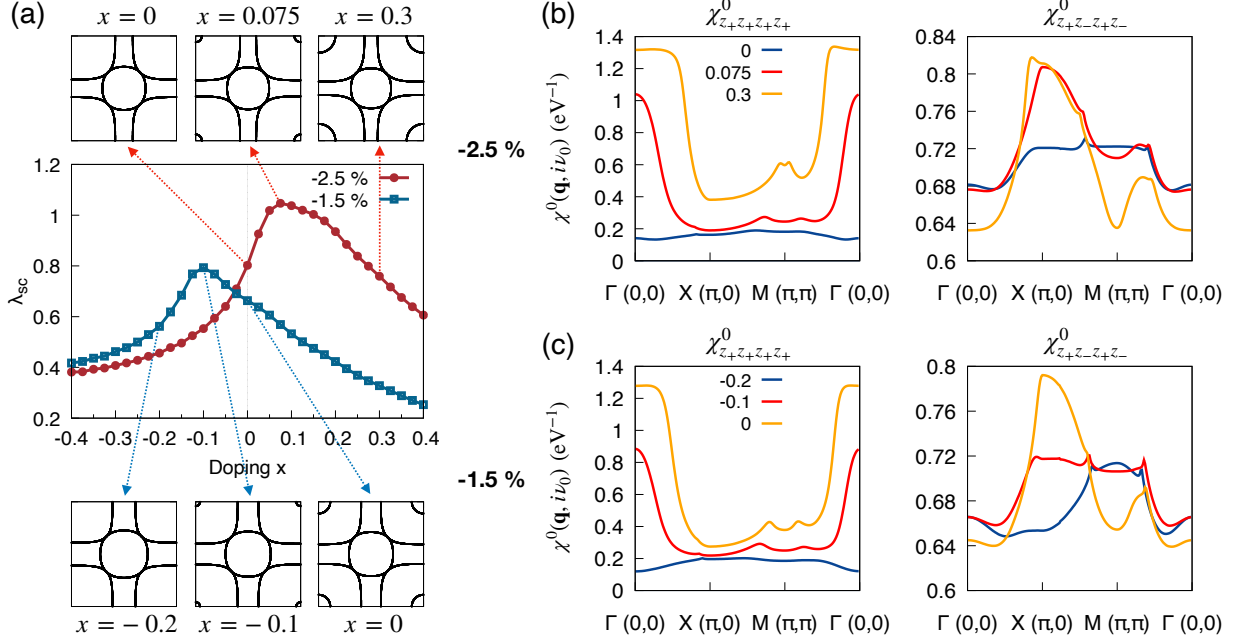


FIG. S5. (a) The leading λ_{sc} (s_{\pm} -wave pairing) as a function of doping x for -2.5% and -1.5% strains, and the corresponding FSs for selected cases. $x < 0$ corresponds to electron doping and $x > 0$ to hole doping. (b,c) The pair-breaking susceptibility $\chi_{z_+z_+z_+z_+}^0(q, iv_0)$ (left) and pair-forming susceptibility $\chi_{z_+z_-z_+z_-}^0(q, iv_0)$ (right) for several hole doping levels at (b) -2.5% strain and (c) -1.5% strain. $U = 0.96$ eV, $J = U/6$, and $V = 0$.

- [S1] G. Kresse and J. Hafner, *Phys. Rev. B* **47**, 558–561 (1993).
- [S2] G. Kresse and J. Furthmüller, *Comput. Mater. Sci.* **6**, 15 (1996).
- [S3] G. Kresse and J. Furthmüller, *Phys. Rev. B* **54**, 11169–11186 (1996).
- [S4] Y.-F. Zhao and A. S. Botana, *Phys. Rev. B* **111**, 115154 (2025).
- [S5] L. Bhatt, A. Y. Jiang, E. K. Ko, N. Schnitzer, G. A. Pan, D. F. Segedin, Y. Liu, Y. Yu, Y.-F. Zhao, E. A. Morales, C. M. Brooks, A. S. Botana, H. Y. Hwang, J. A. Mundy, D. A. Muller, and B. H. Goode, *Resolving structural origins for superconductivity in strain-engineered $La_3Ni_2O_7$ thin films* (2025), arXiv:2501.08204 [cond-mat.supr-con].
- [S6] J. P. Perdew, K. Burke, and M. Ernzerhof, *Phys. Rev. Lett.* **77**, 3865 (1996).
- [S7] A. A. Mostofi, J. R. Yates, G. Pizzi, Y.-S. Lee, I. Souza, D. Vanderbilt, and N. Marzari, *Computer Physics Communications* **185**, 2309 (2014).
- [S8] N. Marzari, A. A. Mostofi, J. R. Yates, I. Souza, and D. Vanderbilt, *Rev. Mod. Phys.* **84**, 1419 (2012).
- [S9] N. E. Bickers, Self-consistent many-body theory for condensed matter systems, in *Theoretical Methods for Strongly Correlated Electrons*, edited by D. Sénéchal, A.-M. Tremblay, and C. Bourbonnais (Springer New York, New York, NY, 2004) pp. 237–296.
- [S10] G. Rohringer, H. Hafermann, A. Toschi, A. Katanin, A. Antipov, M. Katsnelson, A. Lichtenstein, A. Rubtsov, and K. Held, *Reviews of Modern Physics* **90**, 025003 (2018), publisher: American Physical Society.
- [S11] R. B. Lehoucq, D. C. Sorensen, and C. Yang, SIAM (1998).
- [S12] J. Linder and A. V. Balatsky, *Rev. Mod. Phys.* **91**, 045005 (2019).
- [S13] W. Xi, S.-L. Yu, and J.-X. Li, *Phys. Rev. B* **111**, 104505 (2025).